https://doi.org/10.20965/jrm.2018.p0397

Paper:

Controller Performance for Quad-Rotor Vehicles Based on Sliding Mode Control

Takayoshi Oba, Mai Bando, and Shinji Hokamoto

Kyushu University
744 Motooka, Nishi-ku, Fukuoka 819-0395, Japan
E-mail: {oba_62, mbando, hokamoto}@aero.kyushu-u.ac.jp

[Received Novermber 20, 2017; accepted April 12, 2018]

This study applies a sliding mode control (SMC) strategy for a robust controller of a quad-rotor vehicle. First, a controller combined with a nested control loop and an SMC is introduced, because a quad-rotor vehicle has only four control inputs although the vehicle has six degrees of freedom. The control performance for the feedback gains in the nested loop is investigated in numerical simulations. Subsequently, the effects of practical system limitations (control cycle and rotor dynamics) on the control performance are examined. Finally, the robust performance of the SMC strategy on a quad-rotor vehicle is discussed.

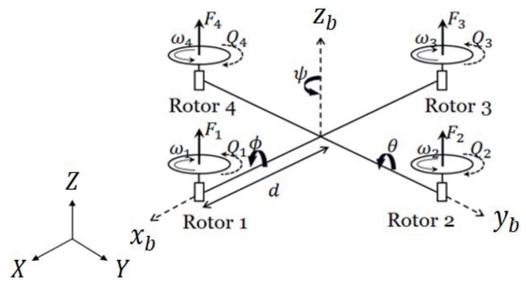

Fig. 1. Model of a quad-rotor vehicle and two frames.

Keywords: sliding mode control, robust control, under-actuated system, quad-rotors

1. Introduction

Recently, numerous missions using micro air vehicles (MAVs) with several rotors have been considered or demonstrated because of their wide application: e.g., in agriculture, industry, military, etc. Quad-rotor vehicles are representatives of MAVs, and their autonomous flight control systems have been actively studied to eliminate humans from operations of dangerous tasks [1–4]. However, quad-rotor vehicles have several problems as flight systems from the control viewpoint. First, they have only four rotors (or control inputs), although they have six degrees of freedom (DOFs); i.e., the system is under-actuated. Second, as their rotor sizes are relatively small compared with single-rotor helicopters, the control force/torque generated by rotors is typically small; that is, their flight stability is not sufficiently large to handle exogenous disturbances. Moreover, the rotor's time constant is relatively large, and the mass balance of vehicles changes according to the onboard payloads. Thus, the flight control systems for quad-rotor vehicles are required to be stable and robust owing to these problems.

To enhance the stability and robustness, this study applies a sliding mode control (SMC) to the autonomous flight control system of a quad-rotor vehicle [5–9]. An SMC is well known to have high robustness for disturbances or modeling errors. However, the SMC's control performance and robustness have not been validated in real control systems for quad-rotor vehicles, owing to the following reasons: in real systems, the time interval in control loops is finite (not infinitesimal) and depends on the hardware. The interval affects the magnitude of "chattering" in the control signals, and the induced chattering typically degrades the behavior of state variables. Meanwhile, the rotors' time constants caused by their dynamics attenuate the quick change in the rotor speeds commanded by the chattering inputs. Furthermore, as quad-rotor vehicles are under-actuated systems, the stability and performance of indirectly controlled variables are not obvious.

Herein, the control strategy combined with an inner loop and the SMC is first introduced to control the six DOFs of a quad-rotor vehicle. The controller performance is investigated in numerical simulations for the specifications of an experimental system in our lab. Subsequently, the effects of the practical system's limitations on control performance are examined, as a preliminary study for future experiments. Finally, the effectiveness of the SMC strategy on a quad-rotor vehicle is discussed.

2. Modeling and Control Strategy

2.1. Mathematical Model of a Quad-Rotor Vehicle

To express a quad-rotor vehicle's motion, we defined two coordinates: a body frame (x_b, y_b, z_b) attached to a vehicle whose origin coincides with the vehicle's mass center, and a world frame (X, Y, Z). **Fig. 1** shows a simple model of a quad-rotor vehicle. We assume that four rotors are placed at a distance d from the mass center and their rotational axes are parallel to the z_b-axis; Rotors 1 and 3 rotate in a counter clockwise direction from the top view, and Rotors 2 and 4 rotate in clockwise; ω_i, F_i and Q_i indicate the rotational speed, thrust force, and reaction torque of the i-th rotor, respectively. The vehicle attitude is defined by the roll-pitch-yaw Euler angles (ϕ, θ, ψ).

A quad-rotor vehicle has six DOFs for its translational and rotational motions. The roll (or pitch) movement about the x_b- (or y_b-) axis is due to the difference between the torques generated by Rotors 1 and 3 (or 2 and 4). The yaw motion about the z_b-axis is generated by the reaction torques of the rotors. Meanwhile, the motion in the z_b-direction is determined by the sum of thrusts of the four rotors, but the x_b- and y_b-directional forces cannot be directly generated by the rotors.

The thrust force and the reaction torque of the i-th rotor are expressed as follows:

$$F_i = b\omega_i{}^2, \tag{1}$$

$$Q_i = -k\omega_i{}^2, \tag{2}$$

where b and k are the lift and reaction coefficients, respectively, and they are assumed to be the same for all the rotors herein. Subsequently, from the geometric relation of the four rotors, the rotational torques and z_b-directional thrust force are defined by each rotor's speed as follows.

$$\begin{bmatrix} T_{xb} \\ T_{yb} \\ T_{zb} \\ F \end{bmatrix} = \begin{bmatrix} db & -db & 0 & 0 \\ 0 & 0 & -db & db \\ k & k & -k & -k \\ b & b & b & b \end{bmatrix} \begin{bmatrix} \omega_1{}^2 \\ \omega_2{}^2 \\ \omega_3{}^2 \\ \omega_4{}^2 \end{bmatrix}, \tag{3}$$

where T_{ib} $(i = x, y, z)$ is the toque, and F is the total force generated by the four rotors. Because the matrix in the right-hand side is non-singular, three rotational torques and one translational force are independently generated through the speed control of the four rotors.

The translational and rotational motions in the world frame of the quad-rotor vehicle are derived from the Newton-Euler formulation as follows. For the translational motion,

$$\begin{cases} \dot{V}_X = \dfrac{F}{m}(\cos\phi\sin\theta\cos\psi + \sin\phi\sin\psi), \\ \dot{V}_Y = \dfrac{F}{m}(\cos\phi\sin\theta\sin\psi - \sin\phi\cos\psi), \\ \dot{V}_Z = -g + \dfrac{F}{m}\cos\phi\cos\theta, \end{cases} \tag{4}$$

where V_i $(i = X, Y, Z)$ is the velocity component in the world frame, m is the vehicle's mass, and g indicates the gravity acceleration. For the rotational motion,

$$\begin{cases} \dot{\omega}_{xb} = \dfrac{I_{yb} - I_{zb}}{I_{xb}}\omega_{yb}\omega_{zb} \\ \qquad + J_r(\omega_1 + \omega_2 - \omega_3 - \omega_4)\,\omega_{yb} + \dfrac{T_{xb}}{I_{xb}}, \\ \dot{\omega}_{yb} = \dfrac{I_{zb} - I_{xb}}{I_{yb}}\omega_{zb}\omega_{xb} \\ \qquad - J_r(\omega_1 + \omega_2 - \omega_3 - \omega_4)\,\omega_{xb} + \dfrac{T_{yb}}{I_{yb}}, \\ \dot{\omega}_{zb} = \dfrac{I_{xb} - I_{yb}}{I_{zb}}\omega_{xb}\omega_{yb} + \dfrac{T_{zb}}{I_{zb}}, \end{cases} \tag{5}$$

where $(\omega_{xb}, \omega_{yb}, \omega_{zb})$ and (I_{xb}, I_{yb}, I_{zb}) are the angular velocities and inertial moments around the principal axes, respectively; J_r indicates the rotor's inertial moment.

For the attitude motion representation of a vehicle, this study adopts quaternion variables [10, 11], because Euler angle representation has singular attitudes and three attitude angles must be stabilized sequentially (not simultaneously). The relation between the angular velocities and time derivatives of the quaternions is expressed by the following equation:

$$\begin{bmatrix} \dot{q}_0 \\ \dot{q}_1 \\ \dot{q}_2 \\ \dot{q}_3 \end{bmatrix} = \frac{1}{2} \begin{bmatrix} 0 & -\omega_{xb} & -\omega_{yb} & -\omega_{zb} \\ \omega_{xb} & 0 & -\omega_{zb} & \omega_{yb} \\ \omega_{yb} & \omega_{zb} & 0 & -\omega_{xb} \\ \omega_{zb} & -\omega_{yb} & \omega_{xb} & 0 \end{bmatrix} \begin{bmatrix} q_0 \\ q_1 \\ q_2 \\ q_3 \end{bmatrix}, \tag{6}$$

2.2. Control Strategy for Translation in World Frame

As described above, the attitude motion around three axes and total force are controlled independently. Thus, the translational forces in the world frame can be generated as the components of the total force by changing the force magnitude and vehicle attitude.

However, quad-rotor vehicles are under-actuated systems, because they have six DOFs. For obtaining or changing the X- (Y-) directional force, the vehicle must change the pitch angle θ (the roll angle ϕ). Thus, to constitute a simple error feedback system, the attitude angles required to reduce the X- and Y-directional position errors can be designed as

$$\begin{cases} \theta_{desire} = K_{PX}X_e + K_{DX}\dot{X}_e, \\ \phi_{desire} = K_{PY}Y_e + K_{DY}\dot{Y}_e, \end{cases} \tag{7}$$

where X_e and Y_e are the position errors, and K_{Pi} and K_{Di} $(i = X, Y)$ are PD gains. This feedback compensation is added as a nested-control loop. Thus, the overall control loop for the quad-rotor vehicle is illustrated in **Fig. 2**. In this figure, $(X_t, Y_t, Z_t, \phi_t, \theta_t, \psi_t)$ indicate the target states of the vehicle, and the angles defined in Eq. (7) are added to θ_t and ϕ_t, respectively. Consequently, θ_t' and ϕ_t' in **Fig. 2** are used instead of θ_t and ϕ_t. Subsequently, the speeds of four rotors are controlled from Eq. (3). It is noteworthy that to achieve both the flight attitude stability and the position error reduction, the feedback gains in Eq. (7) should be selected carefully.

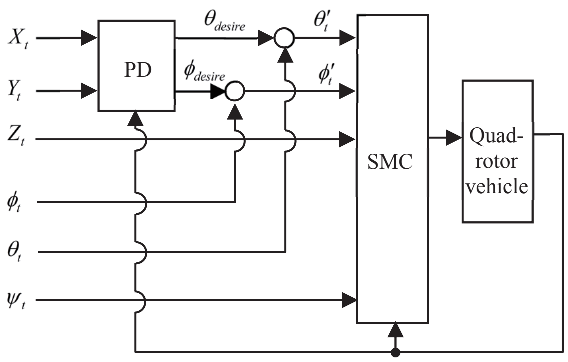

Fig. 2. Control block diagram with a nested loop.

3. Sliding Mode Strategy

3.1. Concept of Sliding Mode Control

The SMC is a type of variable structure control. It is a theory to stabilize a state variable by constraining it onto a pre-defined stable surface, which is called a sliding surface. When the state is constrained on the sliding surface, the state moves to a target point (i.e., the origin of its phase plane) because the surface is stable. The simplest sliding surface is defined by the following equation:

$$S = \dot{x} + \lambda x \quad \dots \dots \dots \dots \quad (8)$$

where λ denotes the slope of the sliding surface, which should be positive for stability.

To move and maintain the state on the sliding surface, the SMC theory typically adopts Lyapunov's second method. The candidate of the Lyapunov function is given with a positive definite function V as follows:

$$\dot{V}(x) < 0 \quad \text{with } V(x) > 0 \quad (\text{for } x \neq 0) \quad \dots \quad (9)$$

Typically, the candidate function is chosen with the distance from the sliding surface as

$$V(x) = \frac{1}{2}S(x)^2 \quad \dots \dots \dots \dots \quad (10)$$

Then, for it to be a Lyapunov function, the function $S(x)$ must satisfy the following relation.

$$\dot{S}(x)S(x) < 0 \quad \dots \dots \dots \dots \quad (11)$$

To guarantee the relation above, the upper limit of the left-hand side value is specified with $-\eta\,|S|$, where η is a positive constant. Then, the state variable x approaches to and remains on the sliding surface for any initial state, when the following relation is satisfied:

$$\ddot{x} + \lambda\dot{x} = -\eta\,\mathrm{sign}(S) \quad \dots \dots \dots \quad (12)$$

Because $\mathrm{sign}(S)$ becomes ± 1 according to the sign of S, the SMC generates the "chattering phenomenon" whenever the state x crosses the sliding surface.

3.2. SMC Controller for the Quad-Rotor Vehicle

The SMC strategy is applied to four variables of the quad-rotor vehicle as shown in **Fig. 2**. As explained in Section 2, three attitude variables and one translational variable can be controlled independently by four control inputs. This means that the SMC controller can be designed separately for these four variables.

Each sliding surface is defined with the tracking error between the desired and current values as follows.

$$\begin{cases} S_{qi} = \dot{q}_{ie} + \lambda_{qi} q_{ie} \quad (i = 1 \sim 3), \\ S_Z = \dot{Z}_e + \lambda_Z Z_e, \end{cases} \quad \dots \quad (13)$$

where q_{ie} denotes the error quaternion for q_i, and Z_e is the tracking error along the Z-direction in the world frame.

Subsequently, according to Eq. (9), the candidates of the Lyapunov functions are set as follows:

$$\begin{cases} V(S_{qi}) = \dfrac{1}{2}{S_{qi}}^2 \quad (i = 1 \sim 3), \\ V(S_Z) = \dfrac{1}{2}{S_Z}^2. \end{cases} \quad \dots \quad (14)$$

Similarly, as described in Section 3.1, the following conditions for the four state variables guarantee that the states approach to and remain on each of the sliding surfaces.

$$\begin{cases} \ddot{q}_{ie} + \lambda_{qi}\dot{q}_{ie} = -\eta_{qi}\mathrm{sign}(S_{qi}) \quad (i = 1 \sim 3), \\ \ddot{Z}_e + \lambda_Z \dot{Z}_e = -\eta_Z \mathrm{sign}(S_Z). \end{cases} \quad (15)$$

Finally, from Eqs. (4) and (5), the control torques for attitude motion and the total lift force can be expressed as follows:

$$\begin{cases} \begin{bmatrix} T_x \\ T_y \\ T_z \end{bmatrix} = \begin{bmatrix} \dfrac{q_0}{I_x} & -\dfrac{q_3}{I_y} & -\dfrac{q_2}{I_z} \\ \dfrac{q_3}{I_x} & \dfrac{q_0}{I_y} & -\dfrac{q_1}{I_z} \\ -\dfrac{q_2}{I_x} & \dfrac{q_1}{I_y} & \dfrac{q_0}{I_z} \end{bmatrix}^{-1} \begin{bmatrix} A_1 \\ A_2 \\ A_3 \end{bmatrix}, \\ F = \dfrac{m}{\cos\phi\cos\theta}\Big(g + \eta_e \mathrm{sign}(S_e) - \lambda_e V_z\Big), \end{cases} \quad (16)$$

where A_1, A_2, and A_3 represent the following equations:

$$\begin{aligned} A_1 &= -2\eta_1\mathrm{sign}(S_1) - 2\lambda_1\dot{q}_1 - \dot{q}_0\omega_x - q_0B_1 \\ &\quad +\dot{q}_3\omega_y + q_3B_2 - \dot{q}_2\omega_z - q_2B_3, \\ A_2 &= -2\eta_2\mathrm{sign}(S_2) - 2\lambda_2\dot{q}_2 - \dot{q}_3\omega_x - q_3B_1 \\ &\quad -\dot{q}_0\omega_y - q_0B_2 + \dot{q}_1\omega_z + q_1B_3, \\ A_3 &= -2\eta_3\mathrm{sign}(S_3) - 2\lambda_3\dot{q}_3 + \dot{q}_2\omega_x + q_2B_1 \\ &\quad -\dot{q}_1\omega_y - q_1B_2 - \dot{q}_0\omega_z - q_0B_3. \\ B_1 &= \frac{I_y - I_z}{I_x}\omega_y\omega_z + \frac{J_r}{I_x}(\omega_1 + \omega_2 - \omega_3 - \omega_4)\omega_y, \\ B_2 &= \frac{I_z - I_x}{I_y}\omega_z\omega_x + \frac{J_r}{I_y}(\omega_1 + \omega_2 - \omega_3 - \omega_4)\omega_x, \\ B_3 &= \frac{I_x - I_y}{I_z}\omega_x\omega_y. \end{aligned}$$

Once the control torques and the total force are obtained from Eq. (16), the speeds of the four rotors are determined from Eq. (3).

4. Numerical Simulations

4.1. Specifications of a Quad-Rotor Vehicle

The parameters of the quad-rotor vehicle used in the numerical simulations are specified based on an experimental system in our laboratory as follows:

$$m = 2.5 \text{ kg},$$
$$\left(I_{xb}, I_{yb}, I_{zb}\right) = (0.0772,\ 0.0764,\ 0.10310) \text{ kgm}^2,$$
$$d = 0.28 \text{ m}, \qquad J_r = 3.4 \times 10^{-5} \text{ kgm}^2,$$
$$b = 5.2 \times 10^{-5} \text{ kgm}^2, \qquad k = 1.1 \times 10^{-6} \text{ kgm}^2.$$

All components of the vehicle's initial states are assumed as zero. The target states are set to $[X_t, Y_t, Z_t, \psi_t] = \left[2\sin(t), 2\cos(t), 2, 0\right]$ as a tracking problem, where t is time. This target trajectory means a circle with a radius of 2 m at an altitude of 2 m. It is noteworthy that for a smooth path tracking, the pitch and roll angles are not specified in the target states.

4.2. Effects of Practical Limitations

In developing practical systems, some limitations caused by hardware performance exist. The control cycle and rotor time constant are the typical ones, and they change the chattering magnitude in SMC. Thus, their effects on controller performance are investigated in numerical simulations.

Nevertheless, the nested control shown in Eq. (7) has been introduced in Section 2, because a quad-rotor is an under-actuated system. Thus, the performance of the nested control loop is first investigated, and then the effects of the practical limitations are examined in numerical simulations.

In all the simulations discussed below, the sampling time interval of the controllers is set to 40 ms except in Section 4.2.2, considering the microprocessor's performance to be used in future experiments. The design parameters in Eq. (15) are set from several numerical trials as follows:

$$\lambda_{qi} = \lambda_Z = 0.3, \quad \eta_{qi} = \eta_Z = 0.4 \quad (i = 1 \sim 3)$$

4.2.1. Effect of the Developed Nested Control Loop

The results shown in **Figs. 3(a)** and **(b)** indicate the vehicle's trajectories in three- and two-dimensional spaces, respectively; **Figs. 3(c)–(e)** and **(f)–(h)** are the time histories of the translational and rotational variables, respectively; **Figs. 3(i)–(l)** are the rotors' speeds. In this simulation, the following three sets of feedback gains are examined:

(i) $K_{PX} = K_{PY} = 0.01$, $K_{DX} = K_{DY} = 0.04$

(ii) $K_{PX} = K_{PY} = 0.04$, $K_{DX} = K_{DY} = 0.04$

(iii) $K_{PX} = K_{PY} = 0.08$, $K_{DX} = K_{DY} = 0.04$

The red, blue, and green lines in the figure indicate the results corresponding to (i)–(iii), respectively. The broken black line means the target trajectory. **Figs. 3(a)–(d)** indicate that some tracking error remains even after the target circle is traced, because the target states are defined with the functions of time.

These results imply the following points: first, the developed nested control loop performs well to control the six state variables of a quad-rotor vehicle. However, unlike the PID control applied to standard systems, larger feedback gains may degrade the tracking performance, and too large gains can easily destabilize the attitude motion for a quad-rotor vehicle. Therefore, the feedback gains should be selected carefully.

From the results above, the feedback gains of the inner loop are set in all the simulations presented below as $K_{PX} = K_{PY} = 0.01$ and $K_{DX} = K_{DY} = 0.04$.

4.2.2. Effect of Sampling Time Interval in Control

In experiments, the sampling time interval in the control loop depends on the controller architecture and hardware. When a microprocessor is onboard a quad-rotor vehicle, the time interval is several tens of milliseconds. If a controller is implemented in a laptop computer outside of a vehicle, the time interval is larger than 100 ms.

Figure 4 indicates the results for the sampling time intervals of 40 ms, 80 ms, and 120 ms in red, blue, and green lines, respectively. The obtained trajectories and the states' time histories are almost the same even when the sampling time interval becomes two or three times 40 ms. However, as shown in **Figs. 4(i)–(l)**, the obvious difference appears in the magnitude of the rotor speeds. This is because the rotor speed increases (decreases) until an updated control command is supplied after one sampling time interval. It should be noted that in this simulation, the time constant of the rotors due to inertia is not considered. (The case including the rotors' time constants shows different results, as shown in Section 4.2.3.)

This result implies that if the rotors' dynamics can be neglected, even a sampling time interval of larger than 100 ms shows a similar result with short time interval cases, except for the magnitude of the rotor speeds.

4.2.3. Effect of the Rotors' Dynamics

In an SMC controller, the control commands are determined discontinuously using signum functions, as shown in Eq. (16). However, the speeds of the four rotors of a vehicle cannot be changed rapidly owing to their inertia. From some preliminary experiments, the rotor's time constant of our experimental system has been identified as approximately 170 ms. Thus, in the simulation, the effects of the rotor time constants of 100 ms and 200 ms are examined and compared with an ideal case of 0-ms time constant.

Figure 5 shows the results for the time constant of 10 ms and 20 ms in blue and green lines, respectively. The red line indicates the result of the ideal case (0 ms). As shown in **Figs. 5(a)–(g)**, the trajectories and the time histories for two cases of the rotor's time constants are almost the same with the ideal case. In **Fig. 5(h)**, the yaw

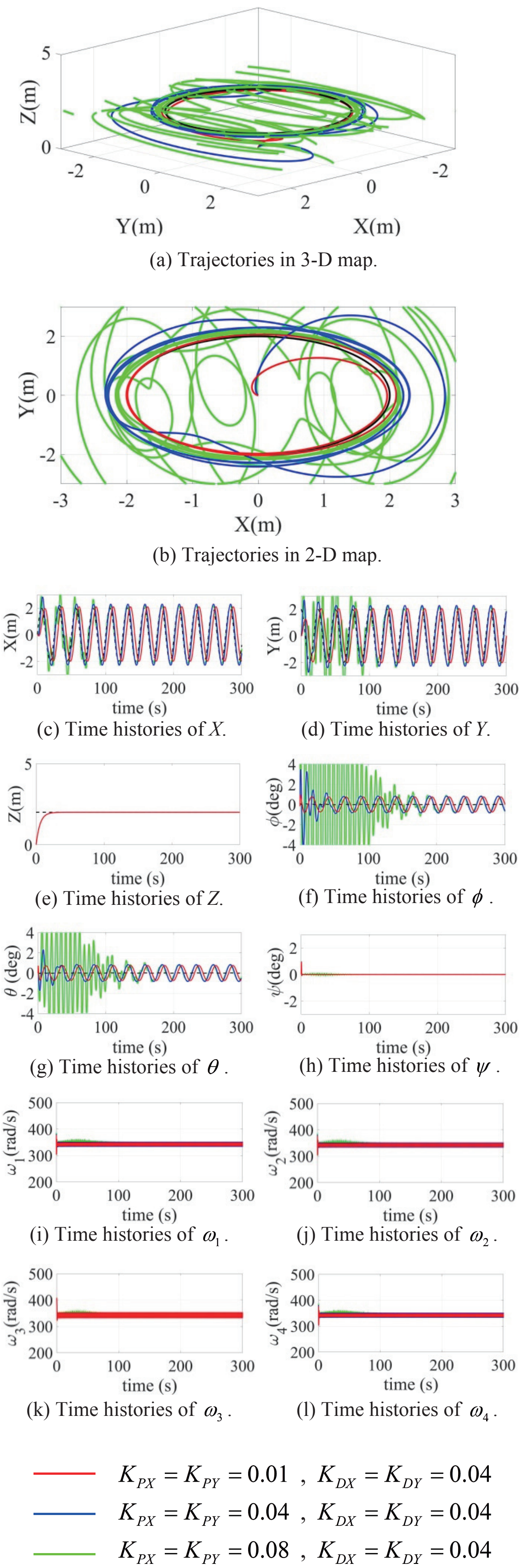

Fig. 3. Effect of the feedback gains in the nested loop.

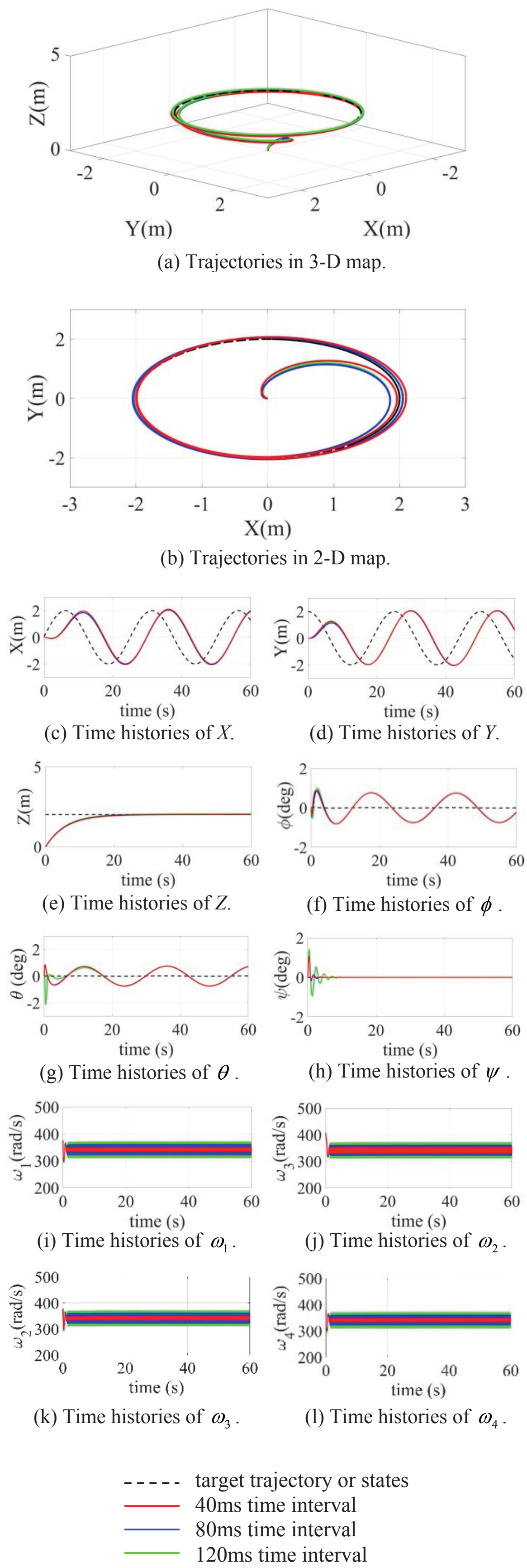

Fig. 4. Effect of the time intervals in the control loop.

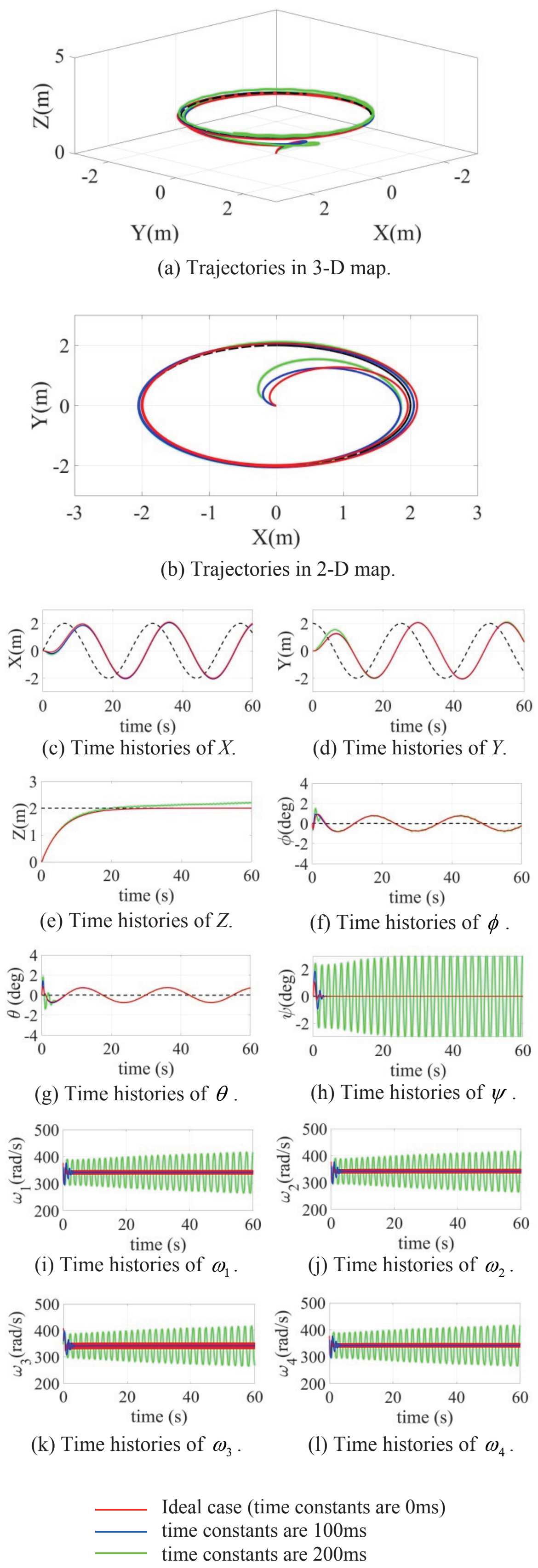

(a) Trajectories in 3-D map.

(b) Trajectories in 2-D map.

(c) Time histories of X.

(d) Time histories of Y.

(e) Time histories of Z.

(f) Time histories of ϕ .

(g) Time histories of θ .

(h) Time histories of ψ .

(i) Time histories of ω_1 .

(j) Time histories of ω_2 .

(k) Time histories of ω_3 .

(l) Time histories of ω_4 .

Fig. 5. Effect of the time constants of the rotors.

angle of the 200 ms case is different from the other two cases, but the error is still small.

Important results are shown in the rotors' histories, **Figs. 5(i)–(l)**: the magnitude of 100 ms case is smaller than that of the 0-ms (ideal case). This is because the rotor's inertia causes a smoother rotational speed. However, the time constant of 200 ms renders the chattering phenomenon worse, and in this simulation the chattering magnitude continues to be larger.

It is noteworthy that the rotors' time constants depend on the rotors and driving motors used in real systems. Once the system is specified, the time constants can be identified. In general, systems with longer time constants have poor stability. However, by adjusting the design parameters λ and η in Eqs. (13) and (15), respectively, the system's stability can be enhanced to a certain extent. Thus, they should be adjusted carefully, considering the trade-off between stability and control performance for the nonlinear dynamics of systems.

4.3. Robust Performance of SMC

The accurate identification of practical vehicles' physical parameters is difficult. Additionally, the payloads of multirotor vehicles change frequently, even in a flight due to dropping or pulling up objects. Thus, the robustness of the developed SMC-based controller on modeling errors is examined herein. In payload change cases, both the mass and inertia moments of the vehicles vary. However, the mass variation changes only the vehicle's translational motion. Thus, this study considers only the effect of inertia moments variations, which may affect the vehicle's flight stability.

4.3.1. Robustness on Modeling Error

First, we solely consider the modeling error; the rotor's time constant is assumed 0 ms, although the sampling time interval of the control is 40 ms. **Fig. 6** shows the results. The blue line indicates the trajectory and states when I_{xb} becomes 10 times of its nominal value. Considering that this change may occur by adding a new payload, I_{zb} $(= I_{xb} + I_{yb})$ is also changed to 5 times of its nominal value. Similarly, the green line is the result when I_{xb} and I_{zb} become 20 times and 10 times from their nominal values, respectively. The red line indicates the result of the nominal model. Even though these are extremely large modeling errors, the developed SMC-based controller is robust against modeling errors.

4.3.2. Robustness Against Modeling Error Considering Rotor Dynamics

For a more realistic condition, the rotor's time constant is assumed as 100 ms, and modeling errors are added to discuss the robustness. **Fig. 7** shows the results. The meaning of the colored lines is the same as those of **Fig. 6**. Compared with **Fig. 6**, the trajectories obtained show a larger overshoot in the altitude response before being settled to a stable condition, and the overshoot is more

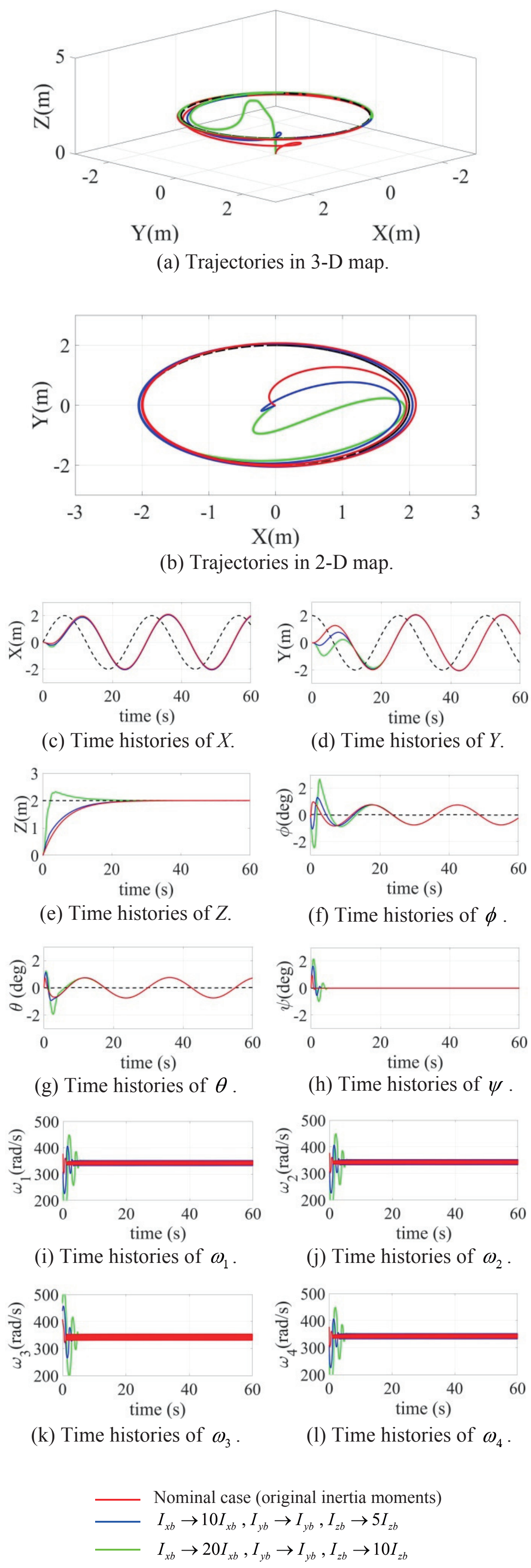

(a) Trajectories in 3-D map.
(b) Trajectories in 2-D map.
(c) Time histories of X.
(d) Time histories of Y.
(e) Time histories of Z.
(f) Time histories of ϕ .
(g) Time histories of θ .
(h) Time histories of ψ .
(i) Time histories of ω_1 .
(j) Time histories of ω_2 .
(k) Time histories of ω_3 .
(l) Time histories of ω_4 .

Fig. 6. Robustness on the modeling errors.

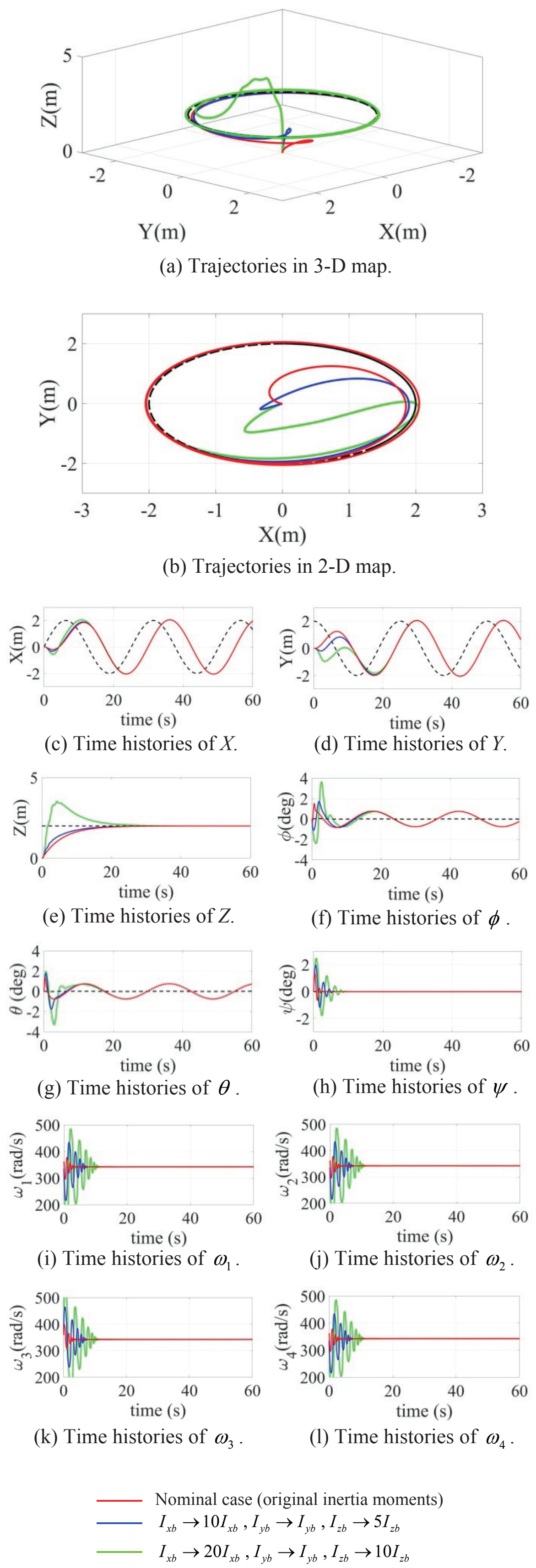

(a) Trajectories in 3-D map.
(b) Trajectories in 2-D map.
(c) Time histories of X.
(d) Time histories of Y.
(e) Time histories of Z.
(f) Time histories of ϕ .
(g) Time histories of θ .
(h) Time histories of ψ .
(i) Time histories of ω_1 .
(j) Time histories of ω_2 .
(k) Time histories of ω_3 .
(l) Time histories of ω_4 .

Fig. 7. Robustness on the modeling errors when the rotors' time constants are assumed to 100 ms.

prominent in the larger modeling error case. Another difference is shown in the rotor's time response. Larger rotor speed variations are shown until 10 s, although the chattering magnitude becomes as small as that in **Fig. 5** for the 100 ms rotor time constant.

Tracking errors are demanded to be as small as possible in various missions. Thus, to reduce the tracking error in Z-axis, the design parameter η_Z in Eq. (15) has changed from 0.4 to 2.0 to increase the control inputs and consequently to enhance the tracking speed to the target altitude. The result of this modification is shown in **Fig. 8**. Red line indicates the modified results ($\eta_Z = 2.0$), and blue line is the original ones ($\eta_Z = 0.4$). As can be seen, the tracking speed of the altitude is much improved, although other states are almost same as **Fig. 7**.

These figures, **Figs. 6–8**, imply that SMC strategy is effective for practical quad-rotor vehicles.

5. Concluding Remarks

This study has applied SMC to control the state variables of a quad-rotor vehicle. As the vehicle has only four control inputs to control its six degrees of freedom, a controller combined with a nested loop and SMC was introduced. The control performance for the feedback gains in the nested loop was investigated in numerical simulations. Then, the effects of practical limitations of the system were examined (the time interval in the control loop and time constant of rotors). Finally, the effectiveness of SMC for an under-actuated quad-rotor vehicle was discussed.

Experimental studies will be carried out by using the results of this study results as a future work.

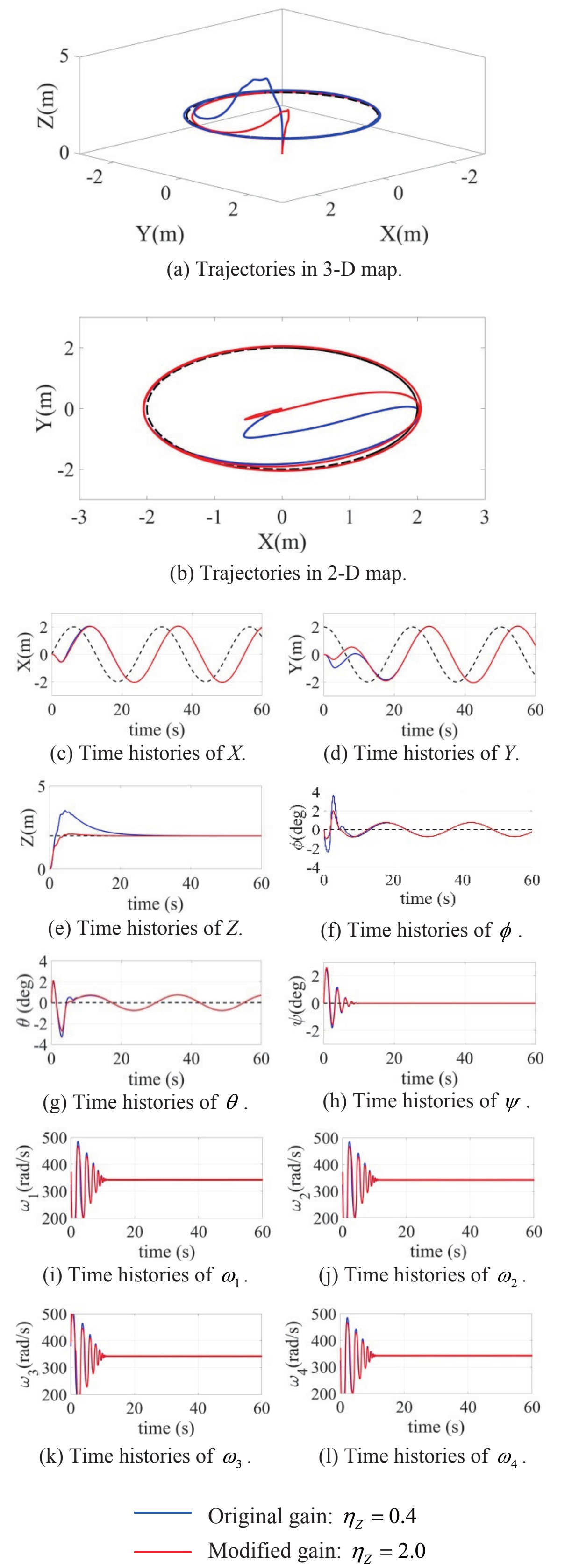

(a) Trajectories in 3-D map.

(b) Trajectories in 2-D map.

(c) Time histories of X. (d) Time histories of Y.

(e) Time histories of Z. (f) Time histories of ϕ.

(g) Time histories of θ. (h) Time histories of ψ.

(i) Time histories of ω_1. (j) Time histories of ω_2.

(k) Time histories of ω_3. (l) Time histories of ω_4.

Fig. 8. Effect of changing in Eq. (15) for a rotors' time constant with 100 ms and a modeling error of $I_{xb} \rightarrow 20I_{xb}$, $I_{yb} \rightarrow I_{yb}$, $I_{zb} \rightarrow 10I_{zb}$.

References:

[1] S. Bouabdallah, A. Noth, and R. Siegwart, "PID vs. LQ Control Techniques Applied to an Indoor Micro Quadrotor," Proc. of the 2004 IEEE/RSJ Int. Conf. on Intelligent Robots and Systems, October 2004, pp. 2451-2456, 2004.

[2] K. Nonami, F. Kendoul, S. Suzuki, W. Wang, and D. Nakazawa, "Development of Autonomous Quad-Tilt-Wing (QTW) Unmanned Aerial Vehicle: Design, Modeling, and Control," Autonomous Flying Robots: Unmanned Aerial Vehicles and Micro Aerial Vehicles, Springer, pp. 77-93, 2010.

[3] D. Droeschel, J. Stuckler, and S. Behnke, "Local Multi-Resolution Surfel Grids for MAV Motion Estimation and 3D Mapping," Proc. of 13th Int. Conf. on Intelligent Autonomous Systems, pp. 429-442, 2014.

[4] S. Islam, J. Dias, and L. D. Seneviratne, "Adaptive tracking control for quadrotor unmanned flying vehicle," Proc. of the 2014 IEEE/ASME Int. Conf. on Advanced Intelligent Mechatronics, pp. 441-445, 2014.

[5] V. Adr, A. Stoica, and J. Whidborne, "Sliding Mode Control of a 4Y Octorotor," UPB Scientific Bulletin, Series D: Mechanical Engineering J., Vol.74, No.4, pp. 37-52, 2012.

[6] E. Zheng, J. Xiong, and J. Luo, "Second Order Sliding Mode Control for a Quadrotor UAV," ISA Trans., Vol.53, No.4, pp. 1350-1356, 2014.

[7] L. Besnard, Y. Shtessel, and B. Landrum, "Quadrotor Vehicle Control via Sliding Mode Controller Driven by Sliding Mode Disturbance Observer," J. of the Franklin Institute, Vol.349, No.2, pp. 658-684, 2012.

[8] N. Ammar, S. Bouallegue, and J. Haggege, "Modeling and Sliding Mode Control of a Quadrotor Unmanned Aerial Vehicle," 3rd Int. Conf. on Automation, Control Engineering and Computer Science, pp. 834-840, 2016.

[9] R. Akbar, B. Sumantri, H. Katayama, S. Sano, and N. Uchiyama, "Reduced-Order Observer Based Sliding Mode Control for a Quad-Rotor Helicopter," J. Robot. Mechatron., Vol.28, No.3, pp. 304-313, 2016.

[10] A. Joshi, A. Kelkar, and J. T.-Y. Wen, "Robust attitude stabilization of spacecraft using nonlinear quaternion feedback," IEEE Trans. on Automatic Control, Vol.40, No.10, pp. 1800-1803, 1995.

[11] E. Stingu and F. Lewis, "Design and implementation of a structured flight controller for a 6dof quadrotor using quaternions," IEEE 17th Mediterranean Conf. on Control and Automation, pp. 1233-1238, 2009.

Name:
Takayoshi Oba

Affiliation:
Web Engineer, Dentsu Kyusyu Inc.

Address:
2-3-13 Meinohamaeki-minami, Nishi-ku, Fukuoka 819-0006, Japan

Brief Biographical History:
2016 Received B.E. from Kyushu University
2018 Received M.E. from Kyushu University
2018- Dentsu Kyusyu Inc.

Main Works:
• "Autonomous Flight of Under-Actuated Quad-Rotor Vehicle Based on Sliding Mode Control," 2017 Asia-Pacific Int. Symposium on Aerospace Technology, Oct., 2017.

Membership in Academic Societies:
• The Japan Society for Aeronautical and Space Sciences (JSAS)

Name:
Mai Bando

Affiliation:
Department of Aeronautics and Astronautics, Kyushu University

Address:
744 Motooka, Nishi-ku, Fukuoka 819-0395, Japan

Brief Biographical History:
2008-2010 Mission Research Fellow, Research Institute for Sustainable Humanosphere, Kyoto University
2010-2012 Assistant Professor, Unit of Synergetic Studies for Space, Kyoto University
2012-2015 Assistant Professor, Department of Aeronautics and Astronautics, Kyushu University
2015- Associate Professor, Department of Aeronautics and Astronautics, Kyushu University

Main Works:
• "Attractive Sets to Unstable Orbits Using Optimal Feedback Control," J. of Guidance, Control, and Dynamics, Vol.39, No.12, pp. 2725-2739, 2016.

Membership in Academic Societies:
• The American Institute of Aeronautics and Astronautics (AIAA)
• The Society of Instrument and Control Engineers (SICE)
• The Japan Society for Aeronautical and Space Sciences (JSASS)

Name:
Shinji Hokamoto

Affiliation:
Professor, Department of Aeronautics and Astronautics, Kyushu University

Address:
744 Motooka, Nishi-ku, Fukuoka 819-0395, Japan

Brief Biographical History:
1987-1992 Research Associate, Department of Mechanical Engineering, Faculty of Science and Engineering, Saga University
1992-1995 Associate Professor, Department of Mechanical Engineering, Faculty of Science and Engineering, Saga University
1996-2010 Associate Professor, Department of Aeronautics and Astronautics, Faculty of Engineering, Kyushu University
2011- Professor, Department of Aeronautics and Astronautics, Faculty of Engineering, Kyushu University

Main Works:
• "Chattering Attenuation Sliding Mode Approach for Nonlinear Systems," Asian J. of Control, Vol.19, No.5, pp. 1-13, 2017.

Membership in Academic Societies:
• The American Institute of Aeronautics and Astronautics (AIAA)
• The Japan Society for Aeronautical and Space Sciences (JSASS)
• The Japan Society of Mechanical Engineering (JSME)
• The Society of Instrument and Control Engineers (SICE)
• The Robotics Society of Japan (RSJ)